Nanomedicine: Nanotechnology, Biology, and Medicine 76 (2026) 102995

Contents lists available at ScienceDirect

Nanomedicine: Nanotechnology, Biology, and Medicine

journal homepage: www.sciencedirect.com/journal/nanomedicine-nanotechnology-biology-and-medicine

Mitochondrial preservation underlies the antioxidant activity of nanoceria particles in light-induced retinal degeneration

Darin Zerti [a,g], Luigi Donato [b,g], Ignacio Babiloni Chust [c], Giulia Carozza [a,h], Omar Giangiulio [a], Marta Stefanini [a], Enver Faella [d], Marco Feligioni [e,f], Jacopo Di Gregorio [a], Vincenzo Flati [a], Matthias Carl [c], Lucia Poggi [c], Rosalia D'Angelo [b], Maurizio Passacantando [d,g], Rita Maccarone [a,*,g]

[a] Department of Biotechnological and Applied Clinical Sciences, University of L'Aquila, 67100, Italy
[b] Department of Biomedical and Dental Sciences and Morphofunctional Imaging, University of Messina, Italy
[c] Department of Cellular, Computational and Integrative Biology (CIBIO), University of Trento, Italy
[d] Department of Physical and Chemical Science, University of L'Aquila, 67100, Italy
[e] Fondazione European Brain Research Institute (EBRI) Rita Levi-Montalcini, Rome, 00161, Italy
[f] Department of Neurorehabilitation Sciences, Casa di cura del Policlinico, 20144, Milan, Italy

ARTICLE INFO

Keywords:
Age-related macular degeneration
Cerium oxide nanoparticles
Mitochondria
Retinal pigment epithelium

ABSTRACT

Age-related Macular Degeneration (AMD), the leading cause of blindness worldwide, is a multifactorial disease with mitochondrial dysfunction recognized as an early pathogenic event. In our preclinical studies, we demonstrated that a single Cerium-Oxide Nanoparticles (CeO_2-NPs) intravitreal injection in a light-induced degeneration model, was able to counteract the retinal degeneration. Our aim was to investigate whether neuroprotection activity could be correlated with mitochondrial morpho-functional preservation. Bulk transcriptomic profiling of whole retinal tissue revealed that light-induced retinal injury was associated with suppression of mitochondrial-related gene networks, including components of the electron transport chain and regulators of mitochondrial dynamics, whereas CeO_2-NPs treatment restored the expression of antioxidant and mitochondrial biogenesis-related genes. Ultrastructural analysis by electron microscopy showed preservation of Retinal Pigmented Epithelial mitochondria's morphology and by high-resolution crystallographic analysis confirmed the intracellular localization of CeO_2-NPs in proximity to mitochondria. Furthermore, Western blot analysis demonstrated that CeO_2-NPs maintained mitophagy markers at basal levels, preventing excessive activation of mitochondrial quality-control pathways. Together, these findings support mitochondrial preservation as a key mechanism underlying nanoceria-mediated retinal neuroprotection and highlight CeO_2-NPs as promising candidates for maintaining retinal homeostasis in AMD.

Introduction

Age Related Macular Degeneration (AMD) represents one of the leading causes of irreversible vision loss worldwide, accounting for approximately 30% of global blindness.[1] Epidemiological projections estimate that by 2040 more than 5.44 million individuals will be affected by AMD, highlighting the growing socio-economic burden associated with this pathology.[1] Despite major advances in understanding retinal degeneration, the molecular mechanisms driving AMD onset and progression remain only partially understood.

The retina is a highly specialized neural tissue responsible for converting light stimuli into electrical signals that are transmitted to the brain via the optic nerve.[2] Photoreceptors, located in the outer retinal layers, are among the most metabolically active neurons in the central nervous system and require substantial amounts of ATP to sustain phototransduction and ionic homeostasis.[3] This extreme metabolic demand makes retinal cells particularly vulnerable to oxidative stress resulting from an imbalance between reactive oxygen species (ROS)

* Corresponding author.
E-mail address: rita.maccarone@univaq.it (R. Maccarone).
[g] These authors contributed equally to this work.
[h] Current address: Biosciences Institute, Newcastle University, Newcastle 1 3BZ, United Kingdom.

https://doi.org/10.1016/j.nano.2026.102995
Received in revised form 30 June 2026;
Available online 16 July 2026
1549-9634/© 2026 The Authors. Published by Elsevier Inc. This is an open access article under the CC BY license (http://creativecommons.org/licenses/by/4.0/).

production and antioxidant defences.[4,5] Mitochondria play a central role in maintaining retinal homeostasis by providing the energy necessary for photoreceptor function while simultaneously regulating cellular redox balance.

Mitochondria are highly dynamic organelles that continuously undergo fusion and fission processes to maintain structural integrity and metabolic efficiency. Together with mitophagy, these processes form the mitochondrial quality-control system[6] that preserves mitochondrial function and limits ROS accumulation.[5,7] Disruption of these mechanisms leads to impaired oxidative phosphorylation, excessive ROS generation and progressive mitochondrial dysfunction. In the retina, this cascade ultimately compromises retinal pigment epithelium (RPE) and photoreceptor survival, contributing to the structural and functional degeneration characteristic of AMD.[8] Indeed, increasing evidence indicates that mitochondrial dysfunction represents one of the earliest pathogenic events during AMD development, particularly in the RPE where high oxygen consumption and metabolic activity render cells especially susceptible to oxidative damage.[9–11]

Given the central role of oxidative stress in retinal degeneration, antioxidant-based therapeutic strategies have gained increasing interest. In this context, nanotechnology has emerged as a promising avenue for developing innovative treatments for neurodegenerative diseases. Cerium Oxide Nanoparticles (CeO_2-NPs), also known as nanoceria, have attracted considerable attention due to their unique redox properties and catalytic antioxidant activity.[12] Their ability to cycle between Ce^{3+} and Ce^{4+} oxidation states allow them to scavenge reactive oxygen species and modulate oxidative stress in biological systems.[13,14] Several studies have demonstrated that CeO_2-NPs exert immunomodulatory and anti-inflammatory effects, contributing to the reduction of oxidative damage while maintaining a favourable safety profile in ocular tissues.[15]

In retinal degeneration models, our previous studies have demonstrated that intravitreal administration of CeO_2-NPs exerts robust neuroprotective effects. Cerium-Oxide Nanoparticles treatment was shown to preserve retinal function, maintain photoreceptor and RPE morphology, reduce lipofuscin accumulation and microglial activation, and attenuate neuroinflammatory responses in light-induced retinal degeneration models.[13,14,16–18] Furthermore, fluorescence-labelled CeO_2-NPs were found to accumulate within the cytoplasm of RPE cells, suggesting their ability to reach intracellular compartments involved in oxidative stress regulation.[14,16] These findings collectively establish nanoceria as a promising neuroprotective strategy for retinal degenerative diseases.

Despite the growing body of evidence supporting the retinal protective effects of CeO_2-NPs, the cellular and subcellular mechanisms underlying this protection remain partially understood. In particular, the potential involvement of mitochondrial preservation and mitochondrial quality-control pathways has not yet been fully clarified. Considering the fundamental role of mitochondrial integrity in retinal survival, understanding whether CeO_2-NPs-mediated neuroprotection involves direct modulation of mitochondrial structure and function represents a crucial step toward elucidating the mechanisms underlying their therapeutic potential.

Recent studies have highlighted the pivotal role of mitochondrial dysfunction in retinal degenerative diseases, particularly in photoreceptors and RPE cells, which rely heavily on oxidative phosphorylation to sustain their high energy demands. Particularly, photoreceptors rely heavily on oxidative phosphorylation to sustain their high energy demands. However, within the metabolic ecosystem of the outer retina, the RPE preferentially utilizes aerobic glycolysis, as characterized by the pioneering studies of Hurley, Philp, and colleagues.[19–21] This specialized metabolic coupling allows the RPE to conserve glucose for the overlying neuroretina while utilizing alternative substrates, such as lactate, for its own metabolic maintenance.

Alterations in mitochondrial architecture or bioenergetic function can initiate a cascade of oxidative stress, impaired metabolism and ultimately neuronal degeneration. Therefore, investigating mitochondrial preservation as a potential mechanism of Cerium-Oxide Nanoparticles-mediated neuroprotection may provide a novel insight linking the antioxidant activity of CeO_2-NPs to retinal protection in AMD.[22,23]

Specifically, we investigated the intracellular localization of CeO_2-NPs within retinal tissue, the morpho-functional alterations occurring in mitochondria during retinal degeneration and whether CeO_2-NPs preserve mitochondrial integrity and mitophagy-related signalling.

Materials and methods

Ethical approval and animal handling

All experiments were conducted in accordance with the ARVO statement for the use of animals in ophthalmic and vision research, authorization number 763/2020-PR by the Italian Ministry of Health and in accordance with European Community Council guidelines (Directive 2014/26/EU). Animals were born and raised in dim cyclic light conditions (12 h light/12 h dark) at constant temperature and relative humidity, provided drinking water and a complete pellet diet (Mucedola, Settimo Milanese, Italy) ad libitum, with an ambient light level of approximately 5 lx. The study was conducted on Albino Sprague-Dawley (SD) rats divided in the following groups:

1) Control animals (CTRL) (n = 12);
2) SD rats + LD+ 7 days of recovery (LD) (n = 12);
3) SD rats + CeO_2-NPs injection + LD+ 7 days of recovery (NPs + LD) (n = 12).

All efforts were made to minimize suffering and reduce the number of animals in accordance with the 3Rs principle.

Light exposure

The SD rats were placed in plexiglass cages individually, dark-adapted overnight and the day after they were exposed to high intensity light at 1000 lx for 24 h from 9 a.m..[24] Immediately after the light damage (LD), the rats returned to dim cyclic conditions.

Intravitreal injection of CeO_2 nanoparticles

The Cerium-Oxide Nanoparticles (CeO_2-NPs) are inorganic nanomaterials characterized by a fluorite crystalline structure and mixed Ce^{3+}/Ce^{4+} valence states, conferring catalytic antioxidant activity through regenerative ROS scavenging. CeO_2 nanoparticles at 2–10 nm were synthesized, as previously described.[12] The intravitreal injection of 2 μL of CeO_2-NPs [1 mM] in 0.9% NaCl in both eyes, as reported by Fiorani[14] and Tisi,[16] were performed 3 days before the LD under anaesthesia. After the surgery session, part of the animals was exposed to high continuous light (24 h, 1000 lx). At the end of the experimental timeline the SD rats were euthanised with inhalation of CO_2.

Transcriptomic profiling and mitochondrial gene analysis

Total RNA was extracted from rat retinal tissues using a TRIzol-based protocol, followed by purification with silica membrane columns (Qiagen RNeasy Mini Kit), as previously reported.[23] RNA integrity was confirmed using an Agilent Bioanalyzer 2100, and only samples with RNA Integrity Number (RIN) > 8.0 were used for sequencing. Library preparation was performed using the NEBNext Ultra II RNA Library Prep Kit, and sequencing was carried out on the Illumina NovaSeq 6000 platform to a depth of approximately 30 million paired-end reads per sample. Reads were trimmed and quality-checked using FastQC and Trimmomatic and aligned to the *Rattus norvegicus* Ensembl reference genome (release Rnor_6.0) using STAR aligner. Gene-level counts were obtained using feature Counts and normalized as Transcripts Per Million (TPM) and Reads Per Kilobase of transcript per Million mapped reads

(RPKM). Differential expression analysis was performed using DESeq2 as the primary pipeline for all results reported in Fig. 1 and Table S2. Raw gene-level count matrices generated by featureCounts were imported into R and analysed with DESeq2[25] to normalize counts, estimate dispersion, and test for differential expression between LD vs CTRL, NPs + LD vs CTRL, and NPs + LD vs LD. To specifically assess the potential effect of the intravitreal injection procedure, additional vehicle-control differential expression analyses were performed for Vehicle +LD vs CTRL and Vehicle +LD vs LD. The corresponding volcano plots are reported in Supplementary Fig. S2, while complete DEG outputs and GO enrichment results are provided in Supplementary Tables S5 and S6, respectively. The analysis included n = 6 independent biological replicates per group. Differential expression was assessed using the Wald test, and p-values were adjusted for multiple testing using the Benjamini–Hochberg false discovery rate (FDR) procedure. Genes were considered significantly differentially expressed when they showed an absolute $\log_2$ fold change ≥ 1 and an adjusted p-value (FDR) ≤ 0.05. An independent edgeR[26] analysis was performed as a sensitivity analysis to verify the robustness of the main DEG patterns, but the figures and tables reported in the manuscript are based on the DESeq2 output. TPM values were used only for visualization purposes, whereas differential expression statistics were calculated from raw count data.[27] Mitochondrial-associated genes were selected using a predefined Gene Ontology (GO)-based annotation strategy. Briefly, genes were classified as mitochondrial-associated if they were annotated to at least one GO Biological Process or Cellular Component term related to mitochondrial structure or function. These included, but were not limited to, mitochondrion and mitochondrial sub-compartment terms, mitochondrial

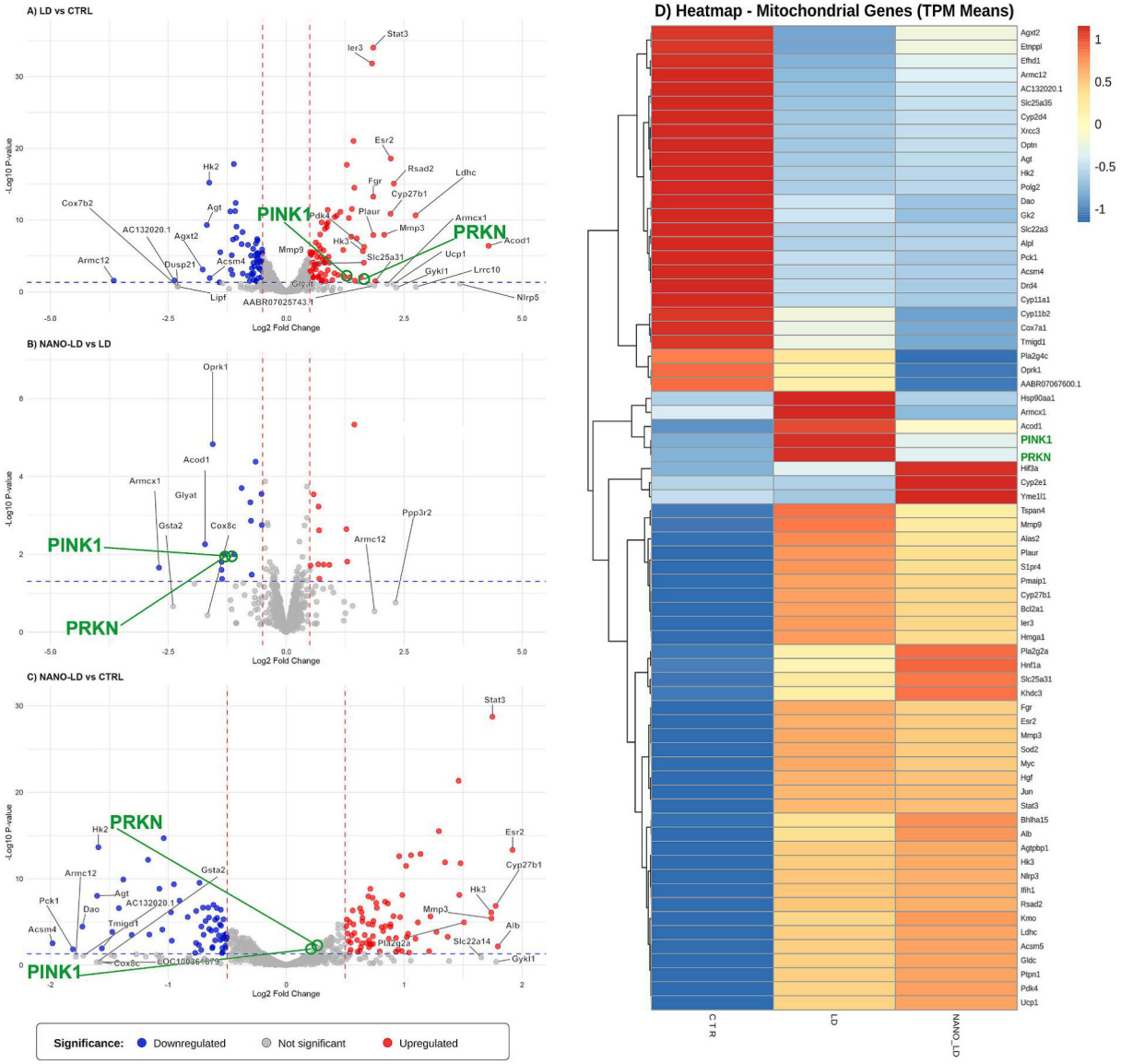


Fig. 1. Transcriptional modulation of mitochondrial genes across experimental groups. (A) Volcano plot for LD vs CTRL. (B) Volcano plot for NPs + LD vs LD. (C) Volcano plot for NPs + LD vs CTRL. Differential expression statistics shown in the volcano plots are based on DESeq2 analysis of raw gene counts; edgeR was used as an independent confirmatory pipeline, and TPM-normalized values were used for heatmap visualization. Significance is defined as $|\log_2 FC| \geq 1$ and FDR (Benjamini–Hochberg) ≤ 0.05; significantly up-regulated genes are shown as filled markers to the right, significantly down-regulated to the left, and non-significant transcripts in faint grey. *PINK1* and *PRKN* are highlighted with high-contrast markers and labels for immediate visibility. (D) Heatmap of row-scaled $\log_2$-expression (*Z*-scores) for mitochondrial-associated genes significant in at least one comparison, clustered by Euclidean distance. Mitochondrial-associated genes were selected using predefined GO Biological Process and Cellular Component annotations related to mitochondrial structure and function. Complete gene-level differential expression outputs, mitochondrial GO annotations, and GO enrichment results are provided in Supplementary Tables S2–S4. Group abbreviations: CTRL; control, LD; light-damage, and NPs + LD; Nanoparticles and light-damage.

membrane and respiratory-chain terms, oxidative phosphorylation, cellular respiration, mitochondrial organization, mitochondrial transport, mitochondrial fission/fusion, mitophagy, and mitochondrial antioxidant response. The GO terms used for classification, together with the corresponding GO identifiers and gene assignments, are reported in Supplementary Table S2.

For each pairwise comparison, the full differential expression output was retained, including gene identifier, gene symbol, base mean expression, $\log_2$ fold change, nominal p-value, adjusted p-value/FDR, and significance status. Complete DEG results are provided in Supplementary Table S3. Mitochondrial-associated DEGs were then obtained by intersecting the complete DEG lists with the predefined mitochondrial-associated GO gene set. Genes were considered significantly differentially expressed when they met the criteria $|\log_2 \text{fold change}| \geq 1$ and FDR ≤ 0.05.

Mitochondrial-associated genes were selected using a predefined Gene Ontology (GO)-based annotation strategy. Genes were classified as mitochondrial-associated when they were annotated to GO terms related to mitochondrial structure or function, including mitochondrial localization and sub compartments, mitochondrial membrane, respiratory-chain activity, oxidative phosphorylation, cellular respiration, mitochondrial organization, mitochondrial transport, mitochondrial fission/fusion, mitophagy, and mitochondrial antioxidant response.

GO enrichment analysis was performed for each pairwise comparison shown in Fig. 1: LD vs CTRL, NPs + LD vs CTRL, and NPs + LD vs LD. Biological Process, Cellular Component and Molecular Function enrichment outputs were retained. For each enriched term, the output included GO identifier, term description, ontology category, number of detected genes, detected gene names, number of differentially expressed genes, differentially expressed gene names, nominal p-value, FDR-adjusted p-value and Bonferroni-adjusted p-value. Full GO enrichment results are reported in Supplementary Table S4. Visualization of results was conducted in Python using Matplotlib and Seaborn for volcano plots and heatmaps.

Tissue preparation for transmission electron microscopy (TEM), high resolution TEM (HRTEM) and scanning TEM (STEM)

Eye samples were collected and quickly washed in phosphate-buffered saline (PBS) 0.1 M. To ensure absolute consistency during sample preparation, the orientation of each eye globe was carefully marked during enucleation to reliably distinguish the dorsal and ventral hemispheres were fixed with 2,5% glutaraldehyde for at minimum 48 h at 4 °C. Following the fixation, the eye cup was dissected under a stereomicroscope using a millimeter-scale grid base to guarantee geometric reproducibility. Retinal fragments were systematically collected from identical coordinates in the fundus: specifically, a dorsal piece centered within the high-susceptibility trigger zone well-known as "hot spot"[28–30] and a corresponding ventral piece sampled at the exact same distance from the optic nerve head. Only these standardized regions were processed for resin embedding, ultramicrotomy, and subsequent ultrastructural analysis. Subsequently, the eye globes were dissected by removing the cornea, lens, vitreous hence the remaining posterior eye globes including retina, RPE, choroid and sclera Retinal samples were then postfixed in 1% osmium tetroxide in dH_2O for 1 h and washed 3 times with PBS. Retinal pieces were then dehydrated in a graded ethanol series (30%, 50%, 70%, 90%, 95% and 100%). For the embedding in EPON resin, samples were incubated first in propylene oxide 2 times for 20 min, then in propylene oxide: EPON (1:1) overnight, EPON resin for 1 h at room temperature and finally EPON for 48 h at 60 °C. Ultramicron slicing was operated using a Leica ULTRACUT R ultramicrotome with a 1.2 mm x1mm retinal pieces. 250 nm slices were cut with a glass knife and stained with toluidine blue to visualize retinal layers in the selected area. Once the area was selected, 70 nm sections were cut using a diamond knife. Imaging was performed with TEM Philips microscope (Philips, Japan) operating at 100 kV accelerating voltage, HRTEM and STEM with the same microscope operating at 300 kV accelerating voltage.

Tissue preparation for scanning electron microscopy (SEM)

The retinal morphology structures were analysed using a field emission scanning electron microscope (FE-SEM, Zeiss Leo 1530) at an accelerating voltage of 2.5 kV. The eye samples were collected and fixed with 2,5% glutaraldehyde for at minimum 48 h at 4 °C. Retinal samples were then postfixed in 1% osmium tetroxide in dH_2O for 1 h (dark place in stirring) and washed 2 times with PBS for 15 min. Retinal pieces were then dehydrated in a graded ethyl alcohol series (30%, 50%, 70%, 95% and 100%). Subsequently the retinal samples were incubated with a 50:50 mixture of hexamethyldisilane (HDMS) and ethyl alcohol for 30 min followed by HDMS 100% overnight. To provide the necessary conductivity, the retinal samples were coated with a thin chromium layer by sputter coating prior to SEM acquisition.

Tissue preparation for mitochondrial imaging

After the tissue preparation for TEM as previously described in the dedicated paragraph, part of the slices was stained by contrast for 9 min with UranyLess followed by 6 min of incubation with lead citrate as an enhancer for heavy metal staining in electron microscopy. After several washes in Milli-Q water the images were acquired by the TEM microscope.

Mitochondrial morphometric analyses

Quantification analysis related to the longitudinal mitochondrial morphometric parameters were performed using the National Institutes of Health (NIH) ImageJ, an open-source image processing software developed to analyse multidimensional scientific microscopy images. A minimum of 70 mitochondria, for each experimental condition, were selected and the total area and perimeter were measured, according to the procedure described by Lam.[31]

Protein extraction

Briefly, eyes were enucleated, and the anterior part (cornea, lens and vitreous) was removed. The remaining tissue (eye cup) was used for protein extractions, as previously reported.[32] Total proteins were extracted using a Dounce Homogenizer and a lysis buffer (50 mM Tris-HCl pH 7.5, 1% Triton X-100, 0.1% SDS, EDTA 5 Mm, supplemented with Halt Protease and Phosphatase Inhibitor Cocktail, Thermo Fisher Scientific, Waltham, MA, USA and QS dH_2O), and left on ice for 30 min. After centrifugation (15,000 rpm for 15 min), the supernatant was collected and stored at −80 °C. Total protein concentration was measured through the Bradford Assay (Bio-Rad Laboratories, Milan, Italy) the total proteins were quantified, according to the manufacturer's instructions.

Western blot

40 μg of proteins were run on a Bolt 4–12% Bis-Tris Plus (Thermo Fisher Scientific, MA, USA) at 200 V for 20 min. The proteins were then transferred to the PVDF membrane (Thermo Fisher Scientific, MA, USA) through an iBlot 2 Dry Blotting System (Invitrogen, Waltham, MA, USA, IB21001). Nonspecific bindings were blocked with 5% non-fat dry milk (Bio-Rad Laboratories, Milan, Italy) in TBST at RT for 1 h; after several washes with TBST the membranes were incubated with the primary antibodies at 4 °C overnight. The following day, the membranes were incubated for 1 h at RT with the secondary antibodies. All the primary and secondary antibodies, as well as their concentrations, are reported in Table S1 in the supplementary section. The membranes were incubated in SuperSignal West Pico Plus (Thermo Fisher Scientific Inc.

Waltham, MA, USA) chemiluminescent substrate and the bands were detected using a ChemiDoc XRSplus imaging system (Bio-Rad Laboratories, Milan, Italy). The optical densities of blot bands were evaluated by ImageLab software (Bio-Rad Laboratories, Milan, Italy) analysis and normalized versus Glyceraldehyde-3-Phosphate Dehydrogenase (GAPDH), used as housekeeping.

Statistical analysis

All statistical tests were performed using SigmaPlot 14.0 Systat software (Palo Alto, CA, USA). The standard errors of all means (SE) were calculated. The first type error was set at 5%. Statistical significance was tested using one-way ANOVA followed by Tukey, Dunn's Methods or Bonferroni post hoc comparison. Different symbols were used (* or #) for the p-value, one symbol <0.05, two symbols = p-value<0.01, three symbols = p-value<0.001, four symbols = p-value<0.0001.

Results

Transcriptomic insights into mitochondrial dysfunction and rescue

Bulk transcriptomic profiling of whole retinal tissue revealed a pronounced alteration of several genes, as previously reported,[23] including genes associated with mitochondrial function in retinas exposed to light-induced damage. For Fig. 1, mitochondrial-associated genes were defined using predefined GO annotations related to mitochondrial structure and function. The complete GO-based mitochondrial gene classification is reported in Supplementary Table S2, complete gene-level differential expression outputs are provided in Supplementary Table S3, and GO Biological Process, Cellular Component and Molecular Function enrichment results are reported in Supplementary Table S4. GO enrichment analysis identified multiple significantly enriched Biological Process, Cellular Component and Molecular Function terms in LD vs CTRL and NPs + LD vs CTRL comparisons after FDR correction. In contrast, the direct NPs + LD vs LD comparison showed only a limited number of significant Biological Process terms and no significant Cellular Component or Molecular Function terms after FDR correction. These enrichment results therefore support a broad tissue-level response to light damage and treatment, while the mitochondrial interpretation is based on the predefined mitochondrial-associated gene signature integrated with ultrastructural and biochemical evidence. In the first comparison, LD vs CTRL as reported in Fig. 1A, volcano plots showed a significant downregulation of mitochondrial genes, including electron transport chain components (*Ndufs2*, *Cox6a2*, *Atp5j*) and regulators of membrane potential and dynamics (*Tomm20*, *Opa1*). In parallel, we observed upregulation of pro-apoptotic mediators including *Bax*, *Aifm1*, and *Casp9*, suggesting activation of the intrinsic cell death pathways. Several genes annotated to mitophagy and mitochondrial quality-control pathways, including *Pink1*, *Park2*, *Clpp* and *Lonp1*, showed reduced expression in LD retinas. Because these data derive from whole retinal tissue, this reduction should be interpreted as a tissue-level mitochondrial-associated signature that may reflect both transcriptional modulation and changes in retinal cellular composition after photoreceptor loss. Examining the NPs + LD vs LD (Fig. 1B) a partial transcriptional rescue was evident, with significant up-regulation of antioxidant defences (*Sod2*, *Prdx3*, *Gpx4*) along with regulators of mitochondrial fusion and cristae architecture (*Mfn2*, *Opa1*). The canonical mitophagy sensors *PINK1* and *PRKN* were further down-regulated relative to LD, implying that mitophagic signalling subsides once mitochondrial integrity is reestablished, as shown in Fig. 1 A–C. These results suggest that pretreatment with CeO_2-NPs not only prevents further damage but may also actively stimulate protective transcriptional programs. The NPs + LD vs CTRL comparison, as shown in Fig. 1C, indicates that stress-response transcripts remain mildly elevated, mitochondrial-related transcripts approached near-normal expression levels, particularly those related to oxidative phosphorylation and reactive oxygen species detoxification. The heatmap (Fig. 1D), based on row-wise *Z*-scores of $\log_2$-transformed expression values for mitochondrial-associated genes significantly modulated in at least one comparison, shows separation between CTRL and LD, with NPs + LD displaying an intermediate profile. The mitochondrial-related genes list is reported in Table S2. Together, these transcriptomic data support the presence of a retinal tissue-level mitochondrial-associated signature altered by light damage and partially normalized in NPs + LD retinas, as previously reported[13,14,16] in addition to further findings presented in this study.

Vehicle-control transcriptomic analysis

To determine whether the intravitreal injection procedure contributed to the observed transcriptional effects, we performed additional vehicle-control analyses. Volcano plots for Vehicle+ LD vs CTRL and Vehicle+ LD vs LD are reported in Supplementary Fig. S2. As expected, Vehicle+ LD vs CTRL retained a broad light-damage-associated transcriptional response. In contrast, the direct Vehicle+ LD vs LD comparison did not show significant GO Biological Process, Cellular Component or Molecular Function enrichment after FDR correction, indicating that vehicle injection did not produce a broad pathway-level transcriptomic signature relative to LD. Only a limited number of mitochondrial-associated genes were significantly modulated in Vehicle+ LD vs LD, supporting the interpretation that the mitochondrial-associated transcriptomic profile observed in NPs + LD animals was not simply attributable to the injection procedure. Complete vehicle-control DEG and GO enrichment outputs are provided in Supplementary Tables S5 and S6.

Retinal morphology evaluated through SEM and TEM

Scanning electron microscopy

Previous studies showed the maintenance of retinal function and morphology in a well-established AMD-like model of light-induced retinal degeneration,[33] after a single intravitreal injection of CeO_2-NPs.[13,14,16,17] Furthermore, by labelling nanoceria particles with fluorescein we demonstrated that after intravitreal injection they reached the subretinal space and the retinal epithelial cells, the site where they carry out their antioxidant activity.[13,14,16] To corroborate this evidence, in this study, we performed further experiments by analysing Scanning Electron Microscopy and Transmission Electron Microscopy to:

a) identify the ultrastructural localization of nanoceria particles;
b) to detect by high magnification the retinal tissue morphology;
c) to perform mitochondrial morphometric analysis.

The experiments were performed by comparing three experimental groups (CTRL, LD and NPs + LD). All the representative images shown in Fig. 2 and Fig. 3 refer to the dorsal retinal region, the specific area called "hot spot", that recapitulates the trigger zone (macula) of human AMD.[13,16,29,30,33] SEM images in Fig. 2 panel A, B and C show the outer retina and RPE of control, LD and NPs + LD. Fig. 2B highlights that the exposure to high light caused a significant loss of the retinal outer layer and RPE architecture compared to control retina (Fig. 2A). In addition, panel B also shows the rosettes, the infolding of the ONL, a typical hallmark of retinal degeneration as previously described.[13,34,35] Conversely in NPs + LD (Fig. 2C) samples all anatomical structures of the photoreceptors, including outer segments, connecting cilia, inner segments and outer nuclear layer are well preserved. Furthermore, the RPE and its interaction with outer segments of photoreceptors are well detectable in NPs + LD and CTRL retina (Fig. 2B; C and Fig. S2).

Transmission electron microscopy

Through the high magnification TEM images, as shown in Fig. 3, the

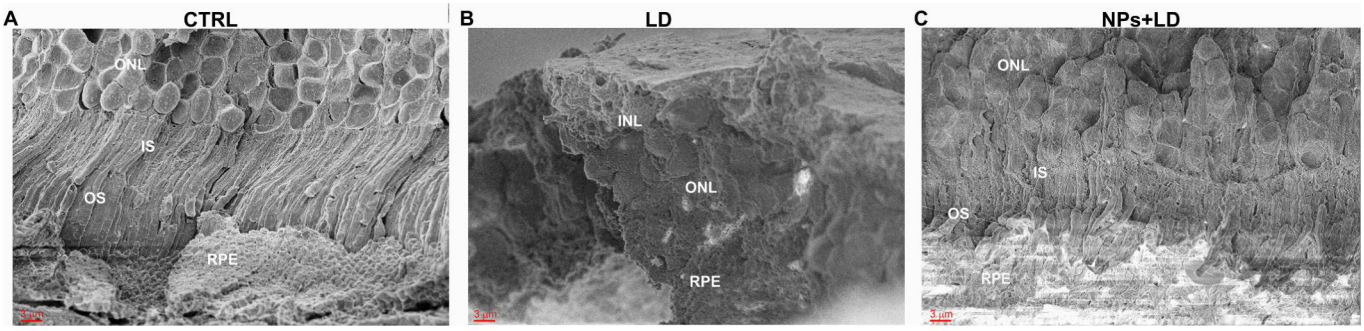


Fig. 2. SEM reveals preservation of photoreceptor and RPE structural organization in nanoceria-treated retinas. Representative images of retinal tissue with SEM, in control retina (panel A), LD (panel B) and NPs + LD (panel C). Abbreviations: RPE; retinal pigmented epithelium; OS; outer segment; CC; connecting cilia; IS; inner segment; ONL; outer nuclear layer; OPL; outer plexiform layer and INL; inner nuclear layer. Scale Bar: 1 μm (A), 3 μm (B) and 2 μm (C). Magnification 5000× (A; B; C).

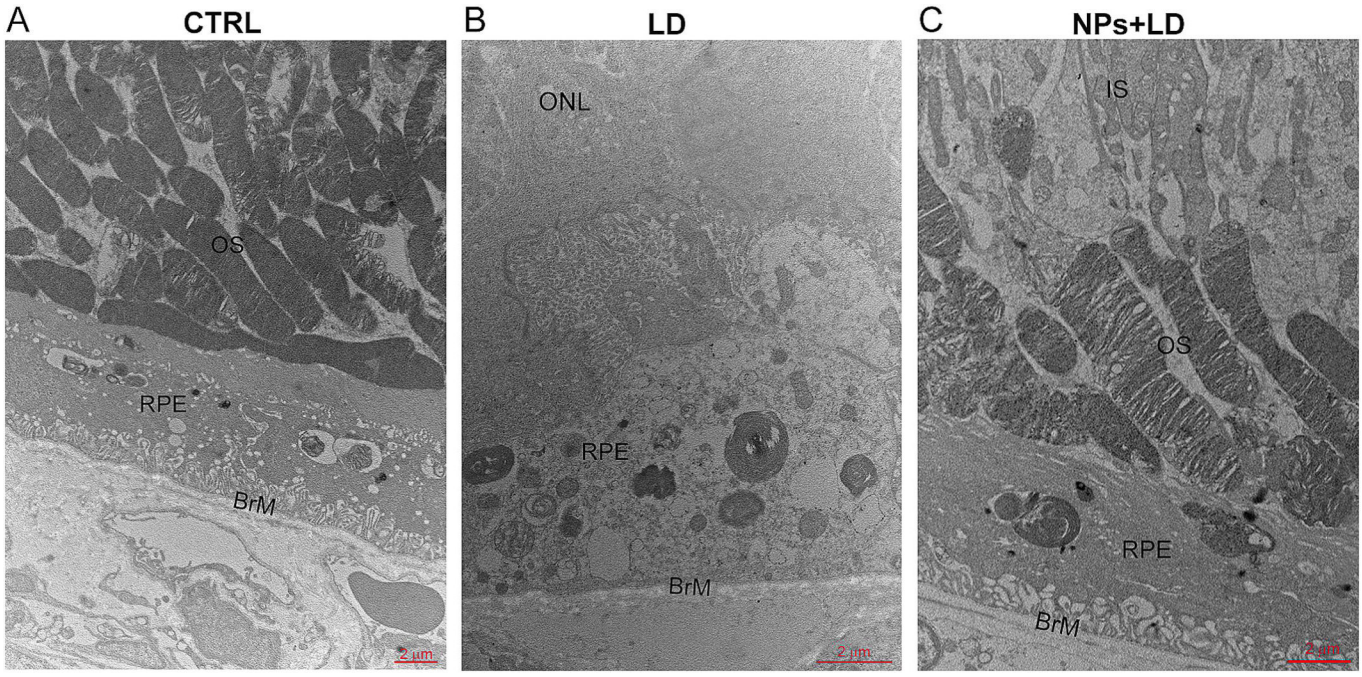


Fig. 3. Ultrastructural comparison of RPE and photoreceptor layers in control, light-damaged, and nanoceria-treated retinas. TEM representative images of outer retina and RPE of control (A), LD (vacuoles, red asterisk) (B) and NPs + LD (C) samples. Abbreviations: RPE; retinal pigmented epithelium; cc; choriocapillaris; OS; outer segment; CC; connecting cilium; IS; inner segment and ONL; outer nuclear layer. Scale Bar: 2 μm (A; B; C). Magnification 3400× (A; B) and 5800× (C).

details of outer retina and RPE can be better appreciated. In the LD group (Fig. 3B) the outer segments of photoreceptors are lost and just a few PR rows in the ONL are still detectable. In addition, intracellular vacuoles along with membranous debris, previously described by Dong[36] et al., are commonly seen in the RPE layer (Fig. 3B, red asterisk), with the hypertrophied subretinal space[37] (Hayden et al., 2021) (Fig. 3B). In control (Fig. 3A) and NPs + LD (Fig. 2C) groups, all cell compartments are well detectable.[38–42] In detail, the ultrastructure images related to the NPs + LD (Fig. 3C) clearly displayed the photoreceptors discs with the connecting cilia and the IS confirming their functional activity as previously demonstrated.[13,14,16] To comprehensively map the spatial progression of the phototoxic lesion and define the exact coordinates of our ultrastructural sampling, a full-length histological reconstruction was performed on a central retinal section passing directly through the optic nerve head (Fig. S3). This central orientation ensures the inclusion of the widest extension of both the dorsal and ventral hemispheres. This low-magnification overview clearly demarcates the focal onset of the degeneration restricted to the highly susceptible dorsal hemisphere, widely described in phototoxicity literature as the regional 'hot spot'. Within this damaged area, the massive loss of photoreceptor rows is accompanied by a severe architectural collapse, characterized by the characteristic infolding of the outer nuclear layer into distinct circular structures, historically referred to as 'rosettes' in acute light-damage models (Fig. S3). To provide a direct multi-scale correlation, Supplementary Fig. 3 also includes high-resolution TEM and SEM images displaying ultrastructural collapse and the preservation of standard tissue morphology within the ventral hemisphere.

Localization of nanoceria particles in the retinal tissue

Transmission electron microscopy analysis was also performed to evaluate the presence of CeO_2-NPs within the retinal tissue. As shown in Fig. 4A, TEM image, acquired at low magnification, revealed cellular structures in which mitochondria (membrane-bound structures) are recognizable, suggesting the integrity of the organelles. Within the

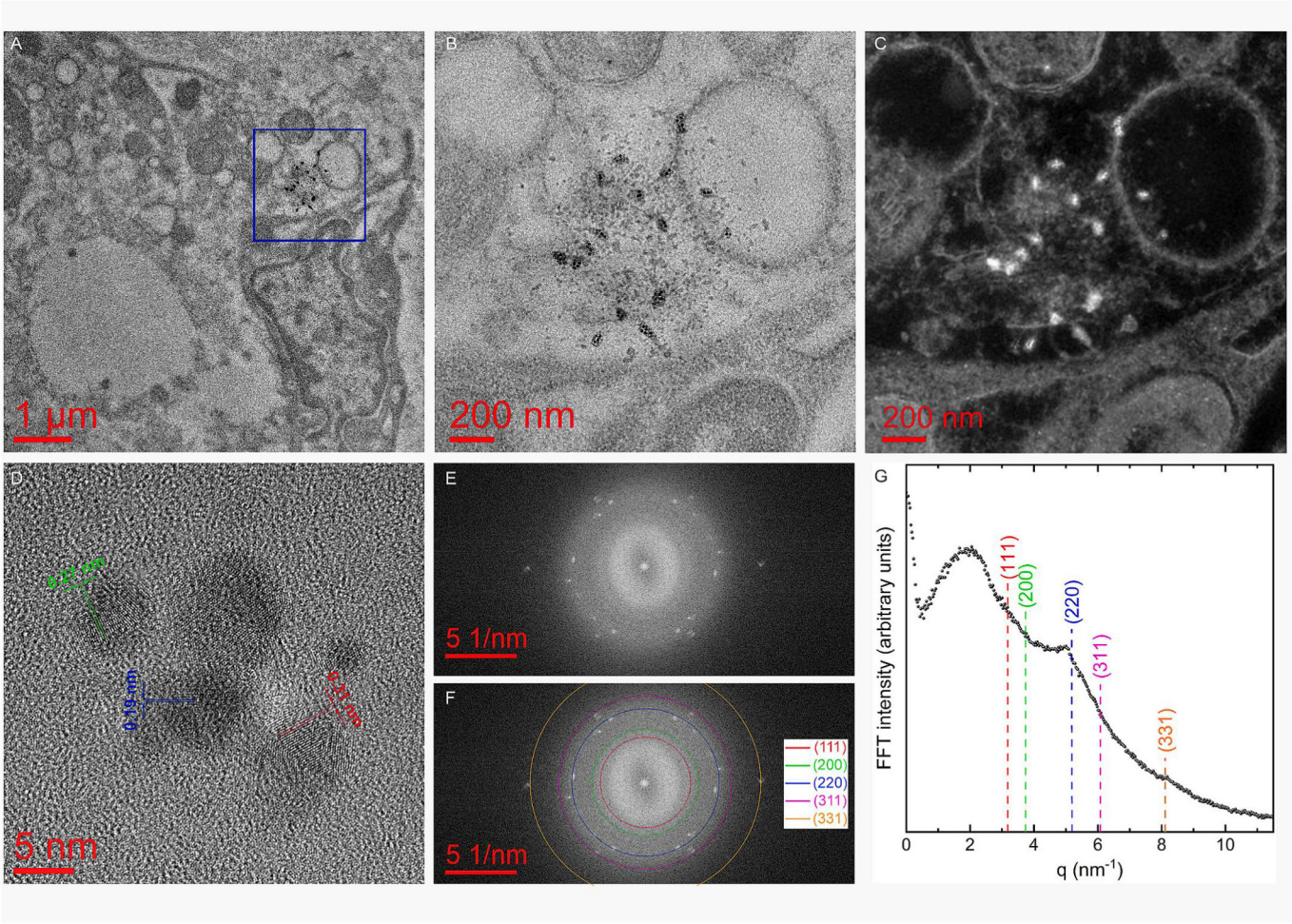


Fig. 4. TEM and HRTEM analysis confirming the localization of CeO_2 nanoparticles in retinal tissue. (A) TEM image at low magnification showing retinal cells with distinguishable mitochondria, recognizable by their characteristic double membrane. The blue box highlights a region of interest containing electron-dense black spots. (B) Higher magnification TEM of the selected region reveals the presence of numerous electron-dense particles that can be ascribed to the intravitreal injection of the CeO_2-NPs. (C) STEM image of the same region; the bright contrast confirms the presence of high atomic number material, consistent with cerium. (D) High-resolution TEM (HRTEM) image showing crystal lattice. Measured interplanar spacings are 0.31 nm (red), 0.27 nm (green), and 0.19 nm (blue), assigned to the (111), (002), and (022) planes of fluorite-structured CeO_2, respectively. (E) FFT of the HRTEM image showing concentric diffraction rings, indicating a polycrystalline structure. (F) Indexed FFT pattern showing rings corresponding to the reflections of cubic CeO_2 structure. (G) Radial intensity profile derived from the FFT shown in the panel E.

cytoplasmic region, black spots are evident in the highlighted blue square that can be attributed to electron-dense particles. Higher magnification (Fig. 4B) of the blue square revealed the presence of discrete, electron-dense nanoparticles with an average diameter of approximately 10 nm, which showed their accumulation within intracellular vesicles, potentially endosomes or lysosomes. Furthermore, Fig. 4C shows the image of the same region acquired by annular dark field scanning transmission electron microscopy (ADF-STEM) technique, where the bright contrast confirms the presence of high atomic number Z. This high dependence on Z (with contrast approximately proportional to Z^2) makes ADF-STEM a useful way to easily identify small areas of an element with a high Z in a matrix of material with a lower Z. Therefore, considering that cerium has an atomic number Z = 58, which is relatively high, especially compared to the most common biological elements present in the retinal tissue (C, H, O, N, P, S, with Z < 20), providing strong evidence that the observed structures are indeed CeO_2-based.

Fig. 4D shows high resolution TEM (HRTEM) image of the region where the intensely bright nanoparticles are visible in Fig. 4C, showing uniform biological tissue and the embedded nanoparticles with a good overall crystallinity, with measured interplanar spacings of 0.31 nm (red), 0.27 nm (green), and 0.19 nm (blue). These preliminary results can be easily assigned to the cubic fluorite-type structure of CeO_2, space group $Fm\underline{3}m$, in agreement with the standard values (JCPDS 34-394).

In addition to continuing the structural analysis, Fast Fourier transform (FFT) was processed on the total region of the HRTEM (Fig. 4D), obtaining a diffraction pattern of concentric rings, typical of polycrystalline materials (Fig. 4E), and, as reported in Fig. 4F from the indexed coloured circles, we have determined the interplanar spacing d from considering the inverse of the measured reciprocal lattice q from the radial intensity profile reported in Fig. 4G. Considering the cubic structure, the lattice parameter a from the individual planes (hkl) can be calculated as follow:

$$a = d_{hkl}\sqrt{h^2 + k^2 + l^2}.$$

All the results are reported in Table 1.

The excellent agreement between the observed and calculated q-values, together with the absence of additional peaks, unambiguously confirms the cubic fluorite structure ($Fm\underline{3}m$) of CeO_2 with a mean lattice parameter $\underline{a} = 0.5413 \pm 0.0053$ nm, and rules out significant contributions from Ce_2O_3, CeO or other impurity phases. The localization of these CeO_2-NPs near mitochondria suggests potential interactions with

Table 1
Structural parameters of CeO_2 nanoparticles identified in retinal tissue by FFT analysis of HRTEM images. Experimental reciprocal lattice values (q_FFT) and interplanar spacings (d_FFT) are reported alongside reference data for cubic fluorite CeO_2 (JCPDS No. 34-394). The lattice parameter a are calculated for each plane.

(hkl)	d (nm) JCPDS 34–394	$q = \frac{1}{d}$ (nm^{-1}) JCPDS 34–394	q_{FFT} (nm^{-1})	$d_{FFT} = \frac{1}{q_{FFT}}$ (nm)	Lattice parameter a (nm)
(111)	0.312	3.20	3.18	0.314	0.5443
(200)	0.271	3.70	3.74	0.267	0.5342
(220)	0.191	5.23	5.19	0.193	0.5453
(311)	0.163	6.13	6.08	0.165	0.5457
(222)	0.156	6.40			
(400)	0.135	7.39			
(331)	0.124	8.05	8.11	0.123	0.5372

intracellular organelles, which may be relevant for understanding CeO_2-related bioactivity and oxidative stress modulation in retinal tissue.

Mitochondria preservation with NPs

Previously we detected the NPs in the RPE and between the photoreceptors OS,[14] our aim was to evaluate whether the nanoparticles treatment could explain their antioxidant activity by interacting with mitochondria and preserving their function. Importantly, there are strong results in the literature, especially with human donors affected by the AMD, that confirm how defects of RPE mitochondria are involved in AMD pathology,[5,8,43–46] including morphological changes and dysfunction related to retinal diseases.[47] Here, we investigated for the first time whether mitochondrial ultrastructural morphology could be preserved by the NPs. Firstly, we investigated the longitudinal mitochondria morphology located in the same area where we previously detected the NPs (Fig. 4), by focusing on morphometric parameters, such as area and perimeter (Fig. 5A, B), using a standardized approach for analysing TEM images, as previously described.[31] Mitochondrial integrity was well preserved in the NPs injected animals, as reported in Fig. 5, that showed significantly lower RPE mitochondrial area (panel A) and perimeter (panel B) in both CTRL and NPs groups compared to the LD group (Fig. 5 A, B). Representative TEM images of the analysed longitudinal mitochondrial (red dotted lines) are reported in Fig. 5 and in Supplementary Fig. 2 (red asterisks). The physiological shape of mitochondria has been detected in the CTRL and NPs + LD groups (Fig. 5 C, E), with the typical mitochondrial cristae that form the inner membrane[48] and the bilayer membrane.[49] Instead, 7 days after the exposure to high light were observed (Fig. 5 D) several compromised swollen mitochondria, as it occurs during cell apoptosis,[41,50] with the mitochondrial membranes and cristae loss (Fig. 5 D, red asterisks) and partial disintegration.[48,51] Therefore, several round structures with slightly heterogeneous electron density and numerous electron-lucent round structures are visible throughout the cytoplasm (Fig. 5 C, D, E, red arrow). These structures are consistent with electron-lucent vacuolar structures consistent with RPE cellular architecture, early endosomal vesicles (Fig. 5 red arrow), immature vacuoles, or large vacuole contains many degenerated cellular organelles (Fig. 5 C, D, E, indicating with red "V") as commonly reported in RPE cells under metabolic or oxidative adaptation.[38,52–54]

Furthermore, we investigated the process of mitophagy, a key cellular process that selectively removes dysfunctional and aging mitochondria.[5,10,44,52,55,56] Research has identified several molecular mechanisms linked to mitophagy, which play a role in the onset of AMD. One of the most investigated is the PTEN-induced putative kinase protein 1 (PINK1)/Parkin-mediated ubiquitination degradation pathway, responsible for the control of mitochondrial structure and function.[44,57] The PINK1-Parkin-derived pathway of mitophagy is generally activated by ROS[56,57] while in physiological conditions, PINK1 and Parkin are present at low levels in the mitochondrial outer membrane and cytoplasm, respectively.[56,58] To assess the NPs effects on the mitophagy machinery, we quantified both proteins from ubiquitin-mediated mitophagy such as the phosphorylated forms of PINK1 (p-PINK1) and Parkin (p-Parkin). We demonstrated the capability to the CeO_2-NPs to maintain both proteins at the basal level while the exposure to the light caused a significant increase of their phosphorylation (Fig. 5 F, G, H), as a consequence of the enhanced oxidative stress and the impairment of the antioxidant defences.

Discussion

This study provides the first comprehensive molecular and ultrastructural evidence that Cerium Oxide Nanoparticles (CeO_2-NPs) exert neuroprotection in retinal degeneration through direct mitochondrial rescue mechanisms. Transcriptomic analysis revealed that mitochondrial dysfunction represents one of the earliest and most fundamental pathogenic events. Light-induced retinal damage triggers a coordinated collapse of mitochondrial gene networks, encompassing electron transport chain components (*Ndufs2*, *Cox6a2*, *Atp5j*), membrane dynamics regulators (*Opa1*, *Mfn2*) and quality control machinery (*Pink1*, *Park2*). This systematic downregulation, together with activation of the intrinsic apoptotic pathways (*Bax*, *Aifm1*, *Casp9*), identifies early mitochondrial dysfunction as a convergent mechanism underlying retinal degeneration across AMD phenotypes.

The ultrastructural evidence provides compelling support for this early mitochondrial involvement. TEM analysis demonstrated a complete loss of outer retinal architecture in light-damaged samples, with severely swollen mitochondria exhibiting disrupted cristae and compromised membrane integrity. These morphological changes are consistent with previous studies of retinal degeneration[41,48,51] and reflect the progression from mitochondrial dysfunction to structural collapse described in AMD pathogenesis.[8]

Our detailed electron microscopy analysis provided the first comprehensive ultrastructural validation of nanoceria-mediated retinal protection, extending beyond the several protective effects reported in our previous studies.[13,14,16,22] While previous studies demonstrated[13,14,16,17,22,59,60] preservation of retinal function, reduction of drusen formation, prevention of neovascularization and microglial activation and downregulation of inflammatory factors, the TEM and SEM analysis revealed a profound disruption of the outer retinal architecture in the dorsal region following light-induced damage.[13,14,16,17,22,59,60] In damaged retinas, photoreceptor outer segments were largely absent and the interface between the retinal pigment epithelium and photoreceptors appeared severely compromised. In contrast, retinas treated with CeO_2-NPs maintained a well-organized tissue architecture, with clearly recognizable photoreceptor discs, connecting cilia, inner segments and an intact RPE layer. Importantly, this preservation of retinal structure was accompanied by marked differences in mitochondrial morphology. Light damage induced pronounced mitochondrial swelling, reflected by a significant increase in mitochondrial area and perimeter in the RPE. Such alterations are widely recognized hallmarks of mitochondrial dysfunction and early apoptotic processes. Notably, CeO_2-NPs treatment effectively prevented these structural abnormalities, maintaining mitochondrial dimensions comparable to those observed in control retinas. These quantitative morphometric findings indicate that nanoceria preserves mitochondrial structural integrity, preventing the swelling and cristae disorganization typically associated with retinal degeneration. Together, these observations provide ultrastructural evidence supporting mitochondrial preservation as a key component of the retinal neuroprotective action of CeO_2-NPs.

Accordingly, molecular analysis further confirmed activation of mitochondrial quality-control pathways. Light damage significantly increased phosphorylation of PINK1 and PARKIN, reflecting activation

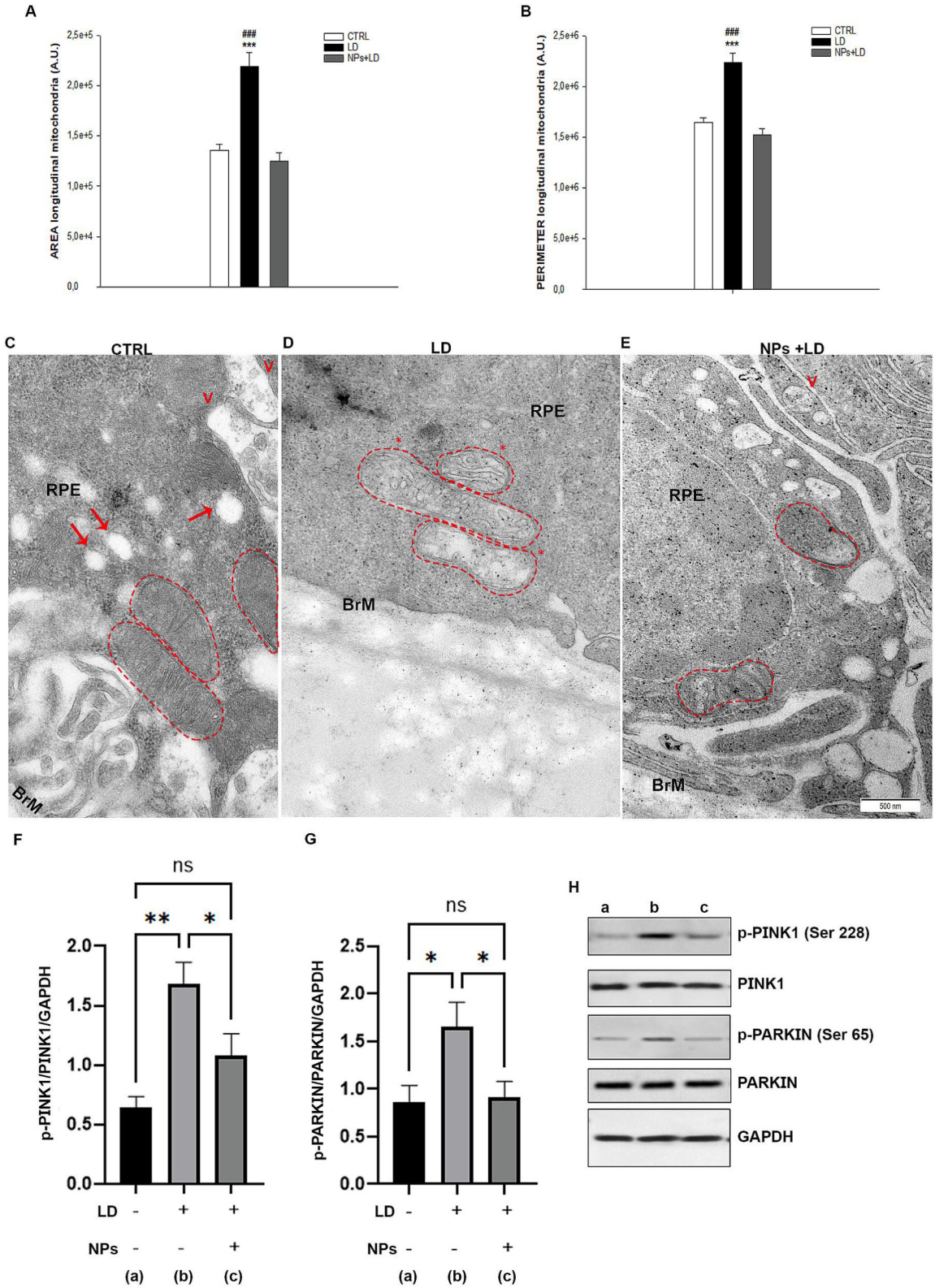


Fig. 5. Nanoceria protects RPE mitochondrial ultrastructure and restores mitophagy signalling. (A–B) Quantification of longitudinal mitochondrial area (A) and perimeter (B) in all experimental groups. Data are shown as mean ± SE. Statistical analysis: one-way ANOVA followed by Dunn's method. ***$p < 0.001$ vs CTRL; $^{###}p < 0.001$ vs LD. (C–E) Representative TEM images of the apical–central region of the RPE cytoplasm in CTRL (C), LD (D) and NPs + LD (E) groups. Red dotted lines indicate mitochondria measured along their longitudinal axis. Red arrows highlight electron-lucent vacuolar structures consistent with RPE cellular architecture, early endosomal vesicles or immature vacuoles. V: vacuole; red asterisk: damaged mitochondria. (F–G) Densitometric analysis of phospho-PINK1/PINK1 (F) and phospho-Parkin/Parkin (G) ratios in retinas from the three groups (a: CTRL; b: LD; c: NPs + LD). Statistical analysis: one-way ANOVA followed by Tukey's test. *$p < 0.05$ vs LD; **$p < 0.01$ vs LD (n = 6). (H) Representative Western blots bands for phospho-PINK1, PINK1, phospho-Parkin, Parkin and GAPDH. Scale bar: 500 nm (C–E).

of stress-induced mitophagy signalling, whereas CeO_2-NPs treatment restored phospho-PINK1 and phospho-PARKIN levels comparable to the control group. These findings indicate that nanoceria prevents PINK1/PARKIN pathway up-regulation, which is well-known to be associated with mitochondrial depolarization and apoptotic cascade.[52,56] Our previous study further supports a disruption of mitochondrial quality-control mechanisms following LD exposure with increased LC3B-II levels while preventing efficient p62 turnover, a pattern indicative of impaired autophagic flux.[16] In contrast, CeO_2-NPs restored LC3B-II and p62 expression to values comparable to controls, reflecting normalization of autophagosome processing.[16] When considered together with the PINK1 and PARKIN phosphorylation profiles, these results demonstrated that nanoceria not only preserves mitochondrial structure but also maintains mitophagy competence and broader autophagic homeostasis under oxidative stress.

High-resolution transmission electron microscopy (HRTEM) combined with crystallographic analysis provided definitive ultrastructural evidence for the presence of CeO_2 nanoparticles within retinal cells. The measured lattice parameter ($\bar{a} = 0.5413 \pm 0.0053$ nm) and interplanar spacings closely matched the theoretical values characteristic of the cubic fluorite structure of Cerium Oxide,[12] confirming the structural identity of the nanoparticles after intravitreal administration and cellular internalization. These findings demonstrate that CeO_2-NPs retain their crystallographic integrity following biological uptake. Importantly, HRTEM imaging revealed the intracellular localization of electron-dense nanoparticles within vesicular compartments near mitochondria, and in several instances directly associated with mitochondrial membranes. This spatial distribution provides direct ultrastructural evidence that nanoceria reach subcellular regions critically involved in oxidative stress regulation and mitochondrial homeostasis. The observed intracellular localization is consistent with previous fluorescence microscopy studies reporting nanoceria accumulation within RPE cells,[14,16] and extends these observations by providing a nanoscale intracellular of distribution. Notably, the proximity of CeO_2-NPs to mitochondria supports the hypothesis that nanoceria may directly contribute to mitochondrial protection by modulating the local redox environment and preserving mitochondrial structural integrity during retinal degeneration. Alternatively, because nanoceria particles act as potent scavengers of ROS, they could blunt the upstream oxidative signalling required to stabilize PINK1 on the outer mitochondrial membrane, thereby impairing the mitophagy surveillance mechanism. However, if nanoceria were simply inhibiting mitophagy irrespective of organelle health, dysfunctional and destroyed mitochondria would accumulate within the cytoplasm due to a blockade in the clearance pathway. On the contrary, our ultrastructural TEM analysis shows no accumulation of degenerated or disrupted mitochondrial profiles in the NPs + LD group, confirming that the baseline levels of PINK1 and Parkin reflect true organelle preservation rather than a compromised surveillance mechanism.

Conclusion

This study establishes mitochondrial rescue as the primary mechanism underlying nanoceria-mediated retinal neuroprotection. The convergent evidence from transcriptomic, ultrastructural and biochemical analyses provides a robust foundation for clinical translation of CeO_2-NPs in retinal degenerative diseases. The targeted preservation of mitochondrial function represents a particularly strategic therapeutic approach, given that mitochondria serve as the primary energy source for the metabolically demanding retinal cells, including photoreceptors and RPE. These cells exhibit among the highest energy requirements in the body, making them critically dependent on optimal mitochondrial performance for survival and function. By preventing early mitochondrial dysfunction, the upstream driver that initiates the cascade toward cellular degeneration, nanoceria-based intervention addresses the fundamental bioenergetic failure that underlies AMD progression across all phenotypes. More broadly, our findings support mitochondrial preservation as a viable therapeutic strategy for neurodegenerative conditions, with nanoceria representing a promising platform for targeted organellar therapy that could prevent disease progression rather than merely treating advanced symptoms.

CRediT authorship contribution statement

Darin Zerti: Writing – original draft, Validation, Investigation, Funding acquisition, Formal analysis, Data curation. **Luigi Donato:** Writing – original draft, Validation, Investigation, Formal analysis, Data curation. **Ignacio Babiloni Chust:** Formal analysis. **Giulia Carozza:** Formal analysis. **Omar Giangiulio:** Formal analysis. **Marta Stefanini:** Formal analysis. **Enver Faella:** Formal analysis. **Marco Feligioni:** Writing – review & editing. **Jacopo Di Gregorio:** Writing – original draft, Formal analysis, Data curation. **Vincenzo Flati:** Writing – review & editing. **Matthias Carl:** Writing – review & editing. **Lucia Poggi:** Writing – review & editing. **Rosalia D'Angelo:** Writing – review & editing, Writing – original draft, Validation. **Maurizio Passacantando:** Writing – review & editing, Writing – original draft, Supervision, Project administration, Funding acquisition, Conceptualization. **Rita Maccarone:** Writing – review & editing, Writing – original draft, Supervision, Project administration, Funding acquisition, Conceptualization.

Consent statement

Not applicable.

Funding

This work was supported by:

- the Ministry of University and Research (MUR, Italy) through the PRIN (Progetti di Rilevante Interesse Nazionale) 2022 grant (ID number: 2022PWMW5A) to R.M.;
- the European Union NextGenerationEU, Mission 4, Component 2, under the Italian Ministry of University and Research (MUR) National Innovation Ecosystem, grant ECS00000041 - VITALITY - CUP E13C22001060006 to M.P.;
- Competitive intramural grants of University of L'Aquila grants number 07_PROGETTO_RICERCA_ATENEO_ZERTI_2022 and 07_PROGETTI_ATENEO_2024 to D.Z. The "Fondazione Umberto Veronesi" supported J.D.G.

Declaration of competing interest

The authors declare no competing interests.

Acknowledgement

We acknowledge Dr. Angelo Sarra for expert assistance with tissue preparation and transmission electron microscopy images acquisition.

Appendix A. Supplementary data

Supplementary data to this article can be found online at https://doi.org/10.1016/j.nano.2026.102995.

Data availability

All relevant data generated during this study are available from the corresponding author upon reasonable request. The raw RNA-seq data (FASTQ files) and processed count matrices have been deposited in the NCBI Gene Expression Omnibus (GEO) under the accession number GSE306375.

References

1. Wong WL, Su X, Li X, Cheung CMG, Klein R, Cheng CY, et al. Global prevalence of age-related macular degeneration and disease burden projection for 2020 and 2040: a systematic review and meta-analysis. *Lancet Glob Health*. 2014;2. https://doi.org/10.1016/S2214-109X(13)70145-1.
2. Casson RJ, Chidlow G, Crowston JG, Williams PA, Wood JPM. Retinal energy metabolism in health and glaucoma. *Prog Retin Eye Res*. 2021;81. https://doi.org/10.1016/J.PRETEYERES.2020.100881.
3. Wang J, Li M, Geng Z, Khattak S, Ji X, Wu D, et al. Role of oxidative stress in retinal disease and the early intervention strategies: a review. *Oxid Med Cell Longev*. 2022;2022. https://doi.org/10.1155/2022/7836828.
4. Eells JT. Mitochondrial dysfunction in the aging retina. *Biology (Basel)*. 2019;8. https://doi.org/10.3390/BIOLOGY8020031.
5. Lakkaraju A, Boya P, Csete M, Ferrington DA, Hurley JB, Sadun AA, et al. How crosstalk between mitochondria, lysosomes, and other organelles can prevent or promote dry age-related macular degeneration. *Exp Eye Res*. 2025;251. https://doi.org/10.1016/j.exer.2024.110219.
6. Chan DC. Mitochondrial dynamics and its involvement in disease. *Annu Rev Pathol*. 2020;15:235–259. https://doi.org/10.1146/ANNUREV-PATHMECHDIS-012419-032711.
7. Chen H, Chan DC. Emerging functions of mammalian mitochondrial fusion and fission. *Hum Mol Genet*. 2005;14(Spec number 2). https://doi.org/10.1093/HMG/DDI270.
8. Kaarniranta K, Uusitalo H, Blasiak J, Felszeghy S, Kannan R, Kauppinen A, et al. Mechanisms of mitochondrial dysfunction and their impact on age-related macular degeneration. *Prog Retin Eye Res*. 2020;79. https://doi.org/10.1016/j.preteyeres.2020.100858.
9. Chichagova V, Hallam D, Collin J, Zerti D, Dorgau B, Felemban M, et al. Cellular regeneration strategies for macular degeneration: past, present and future. *Eye (Lond)*. 2018;32:946–971. https://doi.org/10.1038/S41433-018-0061-Z.
10. Zhang SM, Fan B, Li YL, Zuo ZY, Li GY. Oxidative stress-involved mitophagy of retinal pigment epithelium and retinal degenerative diseases. *Cell Mol Neurobiol*. 2023;43:3265–3276. https://doi.org/10.1007/S10571-023-01383-Z.
11. Nita M, Grzybowski A. Antioxidative role of heterophagy, autophagy, and mitophagy in the retina and their association with the age-related macular degeneration (AMD) etiopathogenesis. *Antioxidants (Basel)*. 2023;12. https://doi.org/10.3390/ANTIOX12071368.
12. Passacantando M, Santucci S. Surface electronic and structural properties of CeO2 nanoparticles: a study by core-level photoemission and peak diffraction. *J Nanopart Res*. 2013;15:1–6. https://doi.org/10.1007/S11051-013-1785-0/FIGURES/6.
13. Tisi A, Passacantando M, Lozzi L, Riccitelli S, Bisti S, Maccarone R. Retinal long term neuroprotection by cerium oxide nanoparticles after an acute damage induced by high intensity light exposure. *Exp Eye Res*. 2019;182:30–38. https://doi.org/10.1016/J.EXER.2019.03.003.
14. Fiorani L, Passacantando M, Santucci S, Di Marco S, Bisti S, Maccarone R. Cerium oxide nanoparticles reduce microglial activation and neurodegenerative events in light damaged retina. *PLoS One*. 2015;10. https://doi.org/10.1371/JOURNAL.PONE.0140387.
15. Cai X, Seal S, McGinnis JF. Non-toxic retention of nanoceria in murine eyes. *Mol Vis*. 2016;22:1176–1187.
16. Tisi A, Flati V, Monache SD, Lozzi L, Passacantando M, Maccarone R. Nanoceria particles are an eligible candidate to prevent age-related macular degeneration by inhibiting retinal pigment epithelium cell death and autophagy alterations. *Cells*. 2020;9:1–17. https://doi.org/10.3390/CELLS9071617.
17. Tisi A, Passacantando M, Lozzi L, Maccarone R. Cerium oxide nanoparticles reduce the accumulation of autofluorescent deposits in light-induced retinal degeneration: insights for age-related macular degeneration. *Exp Eye Res*. 2020;199. https://doi.org/10.1016/j.exer.2020.108169.
18. Tisi A, Passacantando M, Ciancaglini M, Maccarone R. Nanoceria neuroprotective effects in the light-damaged retina: a focus on retinal function and microglia activation. *Exp Eye Res*. 2019;188. https://doi.org/10.1016/j.exer.2019.107797.
19. Kanow MA, Giarmarco MM, Jankowski CSR, Tsantilas K, Engel AL, Du J, et al. Biochemical adaptations of the retina and retinal pigment epithelium support a metabolic ecosystem in the vertebrate eye. *Elife*. 2017;6. https://doi.org/10.7554/ELIFE.28899.
20. Chidlow G, Chan WO, JPM Wood, Casson RJ. Investigations into photoreceptor energy metabolism during experimental retinal detachment. *Front Cell Neurosci*. 2022;16, 1036834. https://doi.org/10.3389/FNCEL.2022.1036834/FULL.
21. Hurley JB, Lindsay KJ, Du J. Glucose, lactate, and shuttling of metabolites in vertebrate retinas. *J Neurosci Res*. 2015;93:1079–1092. https://doi.org/10.1002/JNR.23583.
22. MacCarone R, Tisi A, Passacantando M, Ciancaglini M. Ophthalmic applications of cerium oxide nanoparticles. *J Ocul Pharmacol Ther*. 2020;36:376–383. https://doi.org/10.1089/JOP.2019.0105.
23. Donato L, Zerti D, Babiloni-Chust I, Passacantando M, Flati V, Feligioni M, et al. Comprehensive transcriptomic analysis reveals canonical and novel pathways modulated by nanoceria in mammalian retinal degeneration. *Sci Rep*. 2026. https://doi.org/10.1038/S41598-025-33260-8.
24. Maccarone R, Di Marco S, Bisti S. Saffron supplement maintains morphology and function after exposure to damaging light in mammalian retina. *Invest Ophthalmol Vis Sci*. 2008;49:1254–1261. https://doi.org/10.1167/IOVS.07-0438.
25. Love MI, Huber W, Anders S. Moderated estimation of fold change and dispersion for RNA-seq data with DESeq2. *Genome Biol*. 2014;15. https://doi.org/10.1186/S13059-014-0550-8.
26. Robinson MD, McCarthy DJ, Smyth GK. EdgeR: a Bioconductor package for differential expression analysis of digital gene expression data. *Bioinformatics*. 2010;26:139–140. https://doi.org/10.1093/BIOINFORMATICS/BTP616.
27. Liu S, Wang Z, Zhu R, Wang F, Cheng Y, Liu Y. Three differential expression analysis methods for RNA sequencing: limma, EdgeR, DESeq2. *J Vis Exp*. 2021;2021. https://doi.org/10.3791/62528.
28. Rapp LM, Tolman BL, Koutz CA, Thum LA. Predisposing factors to light-induced photoreceptor cell damage: retinal changes in maturing rats. *Exp Eye Res*. 1990;51:177–184. https://doi.org/10.1016/0014-4835(90)90070-B.
29. Noell WK. Possible mechanisms of photoreceptor damage by light in mammalian eyes. *Vision Res*. 1980;20:1163–1171. https://doi.org/10.1016/0042-6989(80)90055-3.
30. Rutar M, Provis JM, Valter K. Brief exposure to damaging light causes focal recruitment of macrophages, and long-term destabilization of photoreceptors in the albino rat retina. *Curr Eye Res*. 2010;35:631–643. https://doi.org/10.3109/02713681003682925.
31. Lam J, Katti P, Biete M, Mungai M, Ashshareef S, Neikirk K, et al. A universal approach to analyzing transmission electron microscopy with ImageJ. *Cells*. 2021;10. https://doi.org/10.3390/CELLS10092177.
32. Tisi A, Carozza G, Leuti A, Maccarone R, Maccarrone M. Dysregulation of resolvin E1 metabolism and signaling in a light-damage model of age-related macular degeneration. *Int J Mol Sci*. 2023;24. https://doi.org/10.3390/IJMS24076749.
33. Carozza G, Zerti D, Tisi A, Ciancaglini M, Maccarrone M, Maccarone R. An overview of retinal light damage models for preclinical studies on age-related macular degeneration: identifying molecular hallmarks and therapeutic targets. *Rev Neurosci*. 2023;35:303–330. https://doi.org/10.1515/REVNEURO-2023-0130.
34. Flynn E, Ueda K, Auran E, Sullivan JM, Sparrow JR. Fundus autofluorescence and photoreceptor cell rosettes in mouse models. *Invest Ophthalmol Vis Sci*. 2014;55:5643–5652. https://doi.org/10.1167/IOVS.14-14136.
35. Tisi A, Parete G, Flati V, Maccarone R. Up-regulation of pro-angiogenic pathways and induction of neovascularization by an acute retinal light damage. *Sci Rep*. 2020;10. https://doi.org/10.1038/S41598-020-63449-Y.
36. Dong Z, Li J, Leng Y, Sun X, Hu H, He Y, et al. Cyclic intensive light exposure induces retinal lesions similar to age-related macular degeneration in APPswe/PS1 bigenic mice. *BMC Neurosci*. 2012;13. https://doi.org/10.1186/1471-2202-13-34.
37. Hayden CM, Meseck EK. Transmission electron microscopy of the retina: a method for sample preparation and evaluation. *Toxicol Pathol*. 2021;49:521–527. https://doi.org/10.1177/0192623320954124.
38. Samuel Zigler J, Zhang C, Grebe R, Sehrawat G, Hackler L, Adhya S, et al. Mutation in the βA3/A1-crystallin gene impairs phagosome degradation in the retinal pigmented epithelium of the rat. *J Cell Sci*. 2011;124:523–531. https://doi.org/10.1242/JCS.078790.
39. Shang YM, Wang GS, Sliney DH, Yang CH, Lee LL. Light-emitting-diode induced retinal damage and its wavelength dependency in vivo. *Int J Ophthalmol*. 2017;10:191–202. https://doi.org/10.18240/IJO.2017.02.03.
40. Liu X, Zhou Q, Lin H, Wu J, Wu Z, Qu S, et al. The protective effects of blue light-blocking films with different shielding rates: a rat model study. *Transl Vis Sci Technol*. 2019;8. https://doi.org/10.1167/TVST.8.3.19.
41. Brown EE, DeWeerd AJ, Ildefonso CJ, Lewin AS, Ash JD. Mitochondrial oxidative stress in the retinal pigment epithelium (RPE) led to metabolic dysfunction in both the RPE and retinal photoreceptors. *Redox Biol*. 2019;24. https://doi.org/10.1016/j.redox.2019.101201.
42. Naik P, Grebe R, Bhutto IA, Scott Mcleod D, Edwards MM. Histologic and immunohistochemical characterization of GA-like pathology in the rat subretinal sodium iodate model. *Transl Vis Sci Technol*. 2024;13. https://doi.org/10.1167/TVST.13.2.10.
43. Fisher CR, Ferrington DA. Perspective on AMD pathobiology: a bioenergetic crisis in the RPE. *Invest Ophthalmol Vis Sci*. 2018;59:AMD41–7. https://doi.org/10.1167/IOVS.18-24289.
44. Fisher CR, Shaaeli AA, Ebeling MC, Montezuma SR, Ferrington DA. Investigating mitochondrial fission, fusion, and autophagy in retinal pigment epithelium from donors with age-related macular degeneration. *Sci Rep*. 2022;12. https://doi.org/10.1038/S41598-022-26012-5.
45. Terluk MR, Kapphahn RJ, Soukup LM, Gong H, Gallardo C, Montezuma SR, et al. Investigating mitochondria as a target for treating age-related macular degeneration. *J Neurosci*. 2015;35:7304–7311. https://doi.org/10.1523/JNEUROSCI.0190-15.2015.
46. Ferrington DA, Ebeling MC, Kapphahn RJ, Terluk MR, Fisher CR, Polanco JR, et al. Altered bioenergetics and enhanced resistance to oxidative stress in human retinal pigment epithelial cells from donors with age-related macular degeneration. *Redox Biol*. 2017;13:255–265. https://doi.org/10.1016/j.redox.2017.05.015.
47. Tong Y, Zhang Z, Wang S. Role of mitochondria in retinal pigment epithelial aging and degeneration. *Front Aging*. 2022;3. https://doi.org/10.3389/FRAGI.2022.926627.
48. Wang L, Yu X, Zhang D, Wen Y, Zhang L, Xia Y, et al. Long-term blue light exposure impairs mitochondrial dynamics in the retina in light-induced retinal degeneration in vivo and in vitro. *J Photochem Photobiol B*. 2023;240. https://doi.org/10.1016/j.jphotobiol.2023.112654.
49. Feher J, Kovacs I, Artico M, Cavallotti C, Papale A, Balacco Gabrieli C. Mitochondrial alterations of retinal pigment epithelium in age-related macular degeneration. *Neurobiol Aging*. 2006;27:983–993. https://doi.org/10.1016/j.neurobiolaging.2005.05.012.
50. Sun MG, Williams J, Munoz-Pinedo C, Perkins GA, Brown JM, Ellisman MH, et al. Correlated three-dimensional light and electron microscopy reveals transformation of mitochondria during apoptosis. *Nat Cell Biol*. 2007;9:1057–1065. https://doi.org/10.1038/NCB1630.

51. Kwon HJ, Cha MY, Kim D, Kim DK, Soh M, Shin K, et al. Mitochondria-targeting ceria nanoparticles as antioxidants for Alzheimer's disease. *ACS Nano*. 2016;10: 2860–2870. https://doi.org/10.1021/ACSNANO.5B08045.
52. Golestaneh N, Chu Y, Xiao YY, Stoleru GL, Theos AC. Dysfunctional autophagy in RPE, a contributing factor in age-related macular degeneration. *Cell Death Dis*. 2017; 8(1):e2537. https://doi.org/10.1038/cddis.2016.453, 2017;8.
53. Yako T, Otsu W, Nakamura S, Shimazawa M, Hara H. Lipid droplet accumulation promotes RPE dysfunction. *Int J Mol Sci*. 2022;23, 1790. https://doi.org/10.3390/IJMS23031790.
54. Napoli D, Strettoi E. Structural abnormalities of retinal pigment epithelial cells in a light-inducible, rhodopsin mutant mouse. *J Anat*. 2022;243:223. https://doi.org/10.1111/JOA.13667.
55. Wai T, García-Prieto J, Baker MJ, Merkwirth C, Benit P, Rustin P, et al. Imbalanced OPA1 processing and mitochondrial fragmentation cause heart failure in mice. *Science*. 2015;350. https://doi.org/10.1126/SCIENCE.AAD0116.
56. Pinelli R, Lazzeri G, Berti C, Biagioni F, Scaffidi E, Ferrucci M, et al. Retinal autophagy for sustaining retinal integrity as a proof of concept for age-related macular degeneration. *Int J Mol Sci*. 2025;26:5773. https://doi.org/10.3390/IJMS26125773, 2025, Vol 26, Page 5773.
57. Hyttinen JMT, Viiri J, Kaarniranta K, Błasiak J. Mitochondrial quality control in AMD: does mitophagy play a pivotal role? *Cell Mol Life Sci*. 2018;75:2991–3008. https://doi.org/10.1007/S00018-018-2843-7.
58. Yu Y, Wang G, Liu Y, Meng Z. Potential application of traditional Chinese medicine in age-related macular degeneration-focusing on mitophagy. *Front Pharmacol*. 2024; 15. https://doi.org/10.3389/FPHAR.2024.1410998.
59. Schaal KB, Freund KB, Litts KM, Zhang Y, Messinger JD, Curcio CA. OUTER RETINAL TUBULATION IN ADVANCED AGE-RELATED MACULAR DEGENERATION: optical coherence tomographic findings correspond to histology. *Retina*. 2015;35:1339–1350. https://doi.org/10.1097/IAE.0000000000000471.
60. Froines CP, Pak JW, Agrón E, Chew EY, Peto T, Blodi BA, et al. Longitudinal assessment of age-related macular degeneration using ultrawidefield imaging: the optos peripheral retina follow-up study. *Ophthalmology*. 2025;132:569–577. https://doi.org/10.1016/j.ophtha.2024.11.024.